ACS APPLIED MATERIALS & INTERFACES

www.acsami.org

Forum Article

Calcium L-Malate and D-Tartarate Frameworks as Adjuvants for the Sustainable Delivery of a Fungicide

Nurul Farhana Ahmad Aljafree, Mohamad Firdaus Ahmad, Umar Abd Aziz, Mostafa Yousefzadeh Borzehandani, Adila Mohamad Jaafar, Norhayu Asib, Ha L. Nguyen, Mohamed Ibrahim Mohamed Tahir, Muhammad Alif Mohammad Latif, Kyle E. Cordova,* and Mohd Basyaruddin Abdul Rahman*

Cite This: https://doi.org/10.1021/acsami.3c11697

Read Online

ACCESS | Metrics & More | Article Recommendations | Supporting Information

ABSTRACT: Agrichemical adjuvants that combine a highly selective, efficient, and active mode of operation are critically needed to realize a more sustainable approach to their usage. Herein, we report the synthesis and full characterization of two new metal−organic frameworks (MOFs), termed UPMOF-1 and UPMOF-2, that were constructed from eco-friendly Ca^{2+} ions and naturally occurring, low-molecular weight plant acids, L-malic and D-tartaric acid, respectively. Upon structural elucidation of both MOFs, a widely used fungicide, hexaconazole (Hex), was loaded on the structures, reaching binding affinities of −5.0 and −3.5 kcal mol^{-1} and loading capacities of 63% and 62% for Hex@UPMOF-1 and Hex@UPMOF-2, respectively, as a result of the formation of stable host−guest interactions. Given the framework chemistry of the MOFs and their predisposition to disassembly under relevant agricultural conditions, the sustained release kinetics were determined to show nearly quantitative release (98% and 95% for Hex@UPMOF-1 and Hex@UPMOF-2, respectively) after >500 h, a release profile drastically different than the control (>80% release in 24 h), from which the high efficiency of these new systems was established. To confirm their high selectivity and activity, *in vitro* and *in vivo* studies were performed to illustrate the abilities of Hex@UPMOF-1 and Hex@UPMOF-2 to combat the known aggressive pathogen *Ganoderma boninense* that causes basal stem rot disease in oil palm. Accordingly, at an extremely low concentration of 0.05 $\mu g\ mL^{-1}$, both Hex@UPMOF-1 and Hex@UPMOF-2 were demonstrated to completely inhibit (100%) *G. boninense* growth, and during a 26 week *in vivo* nursery trial, the progression of basal stem rot infection was completely halted upon treatment with Hex@UPMOF-1 and Hex@UPMOF-2 and seedling growth was accelerated given the additional nutrients supplied via the disassembly of the MOFs. This study represents a significant step forward in the design of adjuvants to support the environmentally responsible use of agrichemical crop protection.

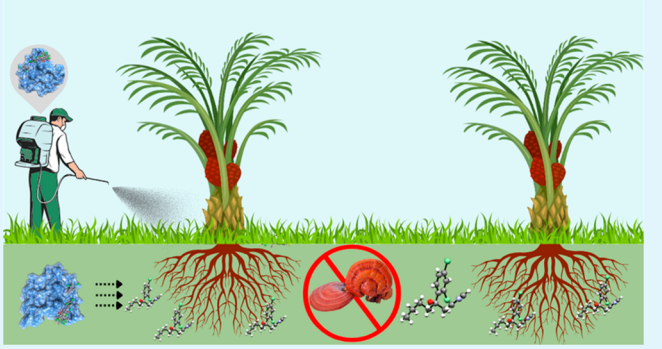

KEYWORDS: *porous materials, agrichemicals, reticular chemistry, delivery systems, crystalline structures*

Downloaded via KING'S COLLEGE LONDON on January 18, 2024 at 07:44:48 (UTC).
See https://pubs.acs.org/sharingguidelines for options on how to legitimately share published articles.

INTRODUCTION

The use of agrichemicals (notably fertilizers and pesticides) in agricultural and non-agricultural settings is directly linked to the well-being of our current and future water, food, health, and environmental systems.[1] Specifically, the improper and inefficient use of such chemicals causes soil erosion and degradation, a decrease in water quality, unintended toxicity to animals (including livestock) and humans upon food consumption, disruption of global nutrient cycles, and increasing energy consumption and greenhouse gas emissions.[2] Though an absolute reduction, if not abstention, in agrichemical usage is necessary, the reality is that these chemicals are heavily relied upon for maintaining and, ultimately, expanding agricultural production to meet societal demands.[3] The grand challenge then in agrichemical development is to develop an adjuvant that is capable of maintaining a high degree of selectivity, efficiency, and activity to minimize off-target effects.[4] An ideal agrichemical adjuvant would witness a targeting mode of operation (selectivity) that reduces reliance on its overusage by decreasing the quantity of the active ingredient while maintaining its overall beneficial properties (efficiency) and by providing positive effects to crop growth, protection, and production (activity).[1,5] From a

Special Issue: Advances in Materials Design and Application

Received: August 8, 2023
Revised: November 24, 2023
Accepted: November 27, 2023

© XXXX American Chemical Society

chemistry point of view, the selectivity is governed by the chemical features of such an adjuvant, efficiency relies on the adjuvant's ability to load appropriate amounts of the active ingredient(s), and activity derives from the adjuvant's structural features and chemical properties.[6]

Herein, we detail two metal−organic frameworks (MOFs) whose structural features and chemical properties afford them with the capability to serve as adjuvants for the selective, efficient, and active delivery of fungicides to combat basal stem rot disease in oil palm. Specifically, we report the synthesis and full characterization of two new MOFs based on eco-friendly Ca^{2+} ions and the naturally occurring, low-molecular weight organic acids, L-malic and D-tartaric acid, termed UPMOF-1 [Ca_3(L-malate)$_3$(H_2O)] and UPMOF-2 [Ca(D-tartrate)], respectively (Figure 1). As a result of their framework

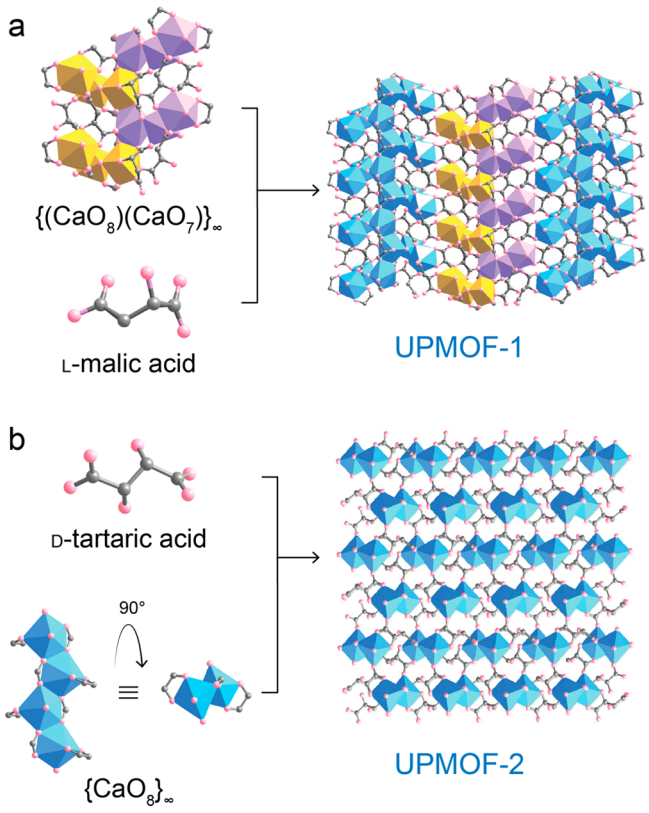

Figure 1. Crystal structures of (a) UPMOF-1 and (b) UPMOF-2 were realized by linking infinite rods of either $\{(CaO_8)(CaO_7)\}_\infty$ or $\{CaO_8\}_\infty$ with the multidentate L-malic acid or D-tartaric acid linkers, respectively. Atom colors: Ca, colored polyhedra; C, gray; O, pink. All H atoms have been omitted for the sake of clarity.

chemistry, we demonstrate their ability to load the commercially used, important fungicide hexaconazole (Hex), and the kinetics of their disassembly under relevant environmental conditions, thereby demonstrating the efficiency of this new adjuvant. Furthermore, we establish their targeted mode of operation (selectivity) and their positive effects in not only combating the known aggressive pathogen *Ganoderma boninense* that causes basal stem rot infection in oil palm but also supporting plant growth due to supplementation of Ca^{2+} from the MOFs into the soil (activity). As a result of their prolonged and sustained release profiles, the Hex-loaded UPMOFs, Hex@UPMOF-1 and -2, were shown to completely inhibit *G. boninense* growth (100%) in terms of *in vitro* antifungal activity after 7 days even at extremely low concentrations (0.05 μg mL^{-1}), and during a 26 week *in vivo* nursery trial, disease progression was completely halted and seedling growth was accelerated by providing additional nutrients from the disassembly of the MOFs within the soil. This study represents a significant step forward in designing new agrichemical adjuvants that are eco-friendly, combat disease progression for sustainable crop production, and provide the added benefits of accelerating plant growth and production.

EXPERIMENTAL SECTION

Materials and General Procedures. Calcium acetate monohydrate (99% pure), calcium nitrate tetrahydrate (99% pure), L-malic acid [99% pure; ee = 99% (GLC)], D-tartaric acid [99.5% pure; ee = 97% (GLC)], potato dextrose agar (PDA), *N*,*N*′-dimethylformamide (DMF; 94.0% pure), and ethanol (99.0% pure) were purchased from Sigma-Aldrich. Hexaconazole (95% pure) was purchased from Megwena Synergy Supply. Potato dextrose agar (PDA), malt extract agar (MEA), and malt extract broth (MEB) were purchased from Oxoid (Malaysia). All chemicals were of analytical grade and used as received without further purification. Thermogravimetric analysis (TGA) was performed using a Mettler Toledo instrument at a heating rate of 10 °C min^{-1} from 50 to 800 °C and a N_2 flow rate of 50 mL min^{-1}. Fourier-transform infrared (FT-IR) spectroscopy analysis was carried out using a Thermo Nicolet 6700 FT-IR spectrometer over a wavenumber range of 4000−400 cm^{-1} with >32 cumulative scans. Elemental microanalysis was performed on a CHNS-O Flash EA 1112 Series elemental analyzer. Acetanilide was run as the standard; O_2 was used as the oxidant, and He served as the carrier gas. Field emission scanning electron microscope (FE-SEM) images were obtained using a JEOL JSM-7600F electron microscope under an emission voltage of 5 kV. Scanning electron microscope (SEM) images and energy dispersive X-ray (EDX) spectroscopy data were obtained and measured using a JEOL JSM 6400 electron microscope under an emission voltage of 20 kV. The samples were dried at room temperature for 12 h under vacuum to remove excess solvents prior to imaging. N_2 sorption measurements were taken at 77 K using a Microtrac Belsorp Mini X gas adsorption analyzer.

Synthesis of Calcium L-Malate Framework: UPMOF-1. Calcium acetate monohydrate (0.071 g, 0.40 mmol) and L-malic acid (0.11 g, 0.80 mmol) were dissolved in a 10 mL mixture of ethanol and deionized water [50:50 (*v*:*v*)] in a 12 mL scintillation vial. The resulting solution was sonicated for 20 min and placed in an oven at 120 °C for 72 h. Colorless, rod-shaped crystals formed at the bottom of the vial. The crystals were washed with ethanol (three time per day for 3 days). The washed sample was then activated under a dynamic vacuum (200 mbar) at room temperature. The yield of activated UPMOF-1 was 40.2%. EA Calcd. for UPMOF-1 ($C_{12}H_{11}Ca_3O_{18}$): C, 24.19; H, 3.73. Found: C, 24.76; H, 3.57. FT-IR (KBr, 3500−400 cm^{-1}): 3470 (br), 3029 (br), 1750 (s), 1279 (s), 1020 (m), 958 (w), 756 (m).

Synthesis of Calcium D-Tartrate Framework: UPMOF-2. Calcium nitrate tetrahydrate (0.071 g, 0.4 mmol) and D-tartaric acid (0.060 g, 1.2 mmol) were dissolved in an 8 mL scintillation vial containing 6 mL of DMF and deionized water [50:50 (*v*:*v*)]. The solution was sonicated for 20 min and placed in an oven at 120 °C for 72 h. Colorless, rod-shaped crystals formed at the bottom of the vial. The crystals were washed with ethanol (three times per day for 3 days). The washed sample was then activated under a dynamic vacuum (200 mbar) at room temperature (25 °C). The yield of activated UPMOF-2 was 37.9%. EA Calcd. for UPMOF-2 ($C_4H_4CaO_6$): C, 21.93; H, 4.13. Found: C, 21.30; H, 4.07. FT-IR (KBr, 3500−400 cm^{-1}): 3499 (br), 2741 (br), 1805 (s), 1169 (m), 964 (w), 752 (m).

Synthesis of MOF-1201. The preparation of MOF-1201 was conducted according to a previously reported procedure.[7] Calcium acetate monohydrate (0.071 g, 0.4 mmol) was transferred to a 12 mL

https://doi.org/10.1021/acsami.3c11697
ACS Appl. Mater. Interfaces XXXX, XXX, XXX−XXX

Teflon autoclave glass vial and dissolved in 7 mL of anhydrous ethanol. Then, 0.072 g (0.8 mmol) of L-lactic acid was added to the solution, and the mixture sonicated for 10 min. The sample was placed in an oven at 120 °C for 96 h. Colorless rod crystals formed at the bottom of the vial. The sample was washed with anhydrous ethanol (three times per day for 3 days). The sample was activated under a dynamic vacuum (200 mbar) at room temperature (25 °C).

X-ray Diffraction Analysis. The single-crystal X-ray diffraction (SCXRD) data for UPMOF-1 and UPMOF-2 were collected using an Oxford Diffraction Gemini E diffractometer with monochromatized Cu Kα radiation (λ = 1.5418 Å) and employing an ω scan at 200 K with flowing nitrogen gas. CrysAlis PRO was used to integrate the raw files that were then solved using a novel dual-space algorithm and refined via a full-matrix least-squares method with SHELXTL.[8] The data were enhanced by applying absorption correction with CrysAlis PRO. Molecular graphics were illustrated with Mercury freeware. The powder X-ray diffraction (PXRD) pattern was recorded using a Shidmadzu diffractometer, with a range of 3−40°, by a Cu Kα radiation source (λ = 1.5405 Å) driven at 40 kV and 30 mA. The simulated PXRD patterns were obtained using the Mercury software based on the single-crystal data.[9]

Molecular Docking Simulation of Hexaconazole (Hex). All docking simulations were performed using the crystallographic information files for UPMOF-1 and -2. The unit cells for UPMOF-1 and -2 were both extended to 3 × 3 × 1, which were determined to be large enough supercell structures to perform the docking simulation. The center of the supercell structures was set for the grid box as 50 × 50 × 50 number of points in three dimensions, and a grid spacing of 1.000 Å was set to cover the entire frameworks. Density functional theory (DFT) calculations were carried out using Gaussian 09. Atomic partial charges were calculated by CHarges from ELectrostatic Potentials using a Grid based (CHelpG) method based on the B3LYP/6-31+G(d) level. AutoDock Vina version 1.1.2 was used to implement the automated molecular docking simulation of hexaconazole with the frameworks. Discovery Studio version 16.1 assisted with the detection of the host−guest interactions.

Loading of Hex on UPMOF-1 and -2 (Hex@UPMOF-1 and Hex@UPMOF-2, respectively). The 10 mg mL^{-1} hexaconazole stock solution was prepared by dissolving 1.0 g of pure hexaconazole in 100 mL of ethanol in a 200 mL volumetric flask. The standard solutions were prepared with concentrations of 20, 40, 60, 80, and 100 μg mL^{-1}. A sample of each UPMOF weighing 100 mg was immersed in a 10.0 mg mL^{-1} hexaconazole solution in a Teflon microwave vial. The vial was capped, and the resulting solution was microwaved at 90 °C with 100 W for 3 min.

Quantification of Hex Loading in Hex@UPMOF-1 and -2. The supernatants of Hex@UPMOF-1 and -2 were collected, filtered (0.25 μm pore size), and transferred to a 2 mL amber glass vial. High-performance liquid chromatography (HPLC; Dionex Ultimate 3000, CLMO Technology) was performed to determine the Hex concentration using a diode array detector. The operating conditions were as follows.[10] Water containing 0.5% phosphoric acid and acetonitrile [25:75 (v:v)] were used as the mobile phase with a flow rate of 1.0 mL min^{-1}, a C18 reversed-phase column (4.6 mm × 250 mm, 5.0 μm inside diameter, Waters), and a detection wavelength of 202 nm. The injection volume was set at 20 μL, and the samples were analyzed at room temperature in triplicate. The retention time obtained for Hex was 4.17 min. The loading capacity (LC) and docking efficiency (DE) were quantified as follows:[11] LC = [(total Hex added in UPMOF-1 or -2 − total Hex unloaded)/(total Hex added in UPMOF-1 or -2)] × 100, and DE = [(weight of Hex@UPMOF-1 or -2)/(weight of UPMOF-1 or -2)] × 100.

***In Vitro* Release Studies.** Hex release was carried out in triplicate by placing 50.0 mg of either Hex@UPMOF-1 or -2 in a dialysis tube (MW cutoff of 14 000 Da) and immersed in 50 mL of phosphate buffer (PBS; 0.04 M, pH 7.4), The solution was chosen to imitate the soil condition as the salts are also present in soil. Each sample was continuously stirred at 300 rpm and 25 °C. At selected interval times, a 3.0 mL aliquot of the supernatant was withdrawn from the beaker and replaced with 3.0 mL of a fresh solution. The Hex concentration was then determined using HPLC as described above.

Hex Release Mechanism and Kinetics. The release profile was investigated using five kinetic models (first-order, second-order, Higuchi, Hixson−Crowell, and Ritger and Peppas).[12,13] On the basis of each model, the collected data were plotted to identify the highest coefficient correlation value (r^2). Full kinetic study details can be found in the Supporting Information.

Culturing *G. boninense*. A pathogenic *G. boninense* culture was obtained from the Toxicology Laboratory, Department of Plant Protection, Faculty of Agriculture, Universiti Putra Malaysia. The culture was periodically subcultured in PDA. The PDA medium was prepared by mixing 39.0 g of PDA powder in 1000 mL of distilled water. The culture medium was sterilized in an autoclave at 121 °C for 20 min and then cooled to room temperature. The PDA medium was poured into Petri dishes (diameter of 10 cm). The inoculum was prepared by cutting the *G. boninense* mycelia using a cork borer (diameter of 1 cm) and transferred to the center of the Petri dishes before being incubated at 29 ± 2 °C for 7 days prior to further usage.[14]

***In Vitro* Antifungal Activity Assay against *G. boninense*.** The antifungal efficacy for the inhibition of *G. boninense* was evaluated by mixing PDA with distilled water alone as a control and the hexaconazole-loaded MOFs Hex@MOF-1201, Hex@UPMOF-1, and Hex@UPMOF-2. For the treatment, the PDA medium was prepared by incorporating five different concentrations of Hex@MOF-1201, Hex@UPMOF-1, and Hex@UPMOF-2: 50 and 100 ppb and 1, 5, and 10 ppm in sterilized PDA.[15] Mycelial discs (diameter of 1 cm) of the *G. boninense* culture were placed in the middle of the PDA agar plates. The inoculated plates were sealed and incubated at 28 ± 2 °C for 7 days. Each treatment contained five replicates. The growth of *G. boninense* in the agar plate was measured through radius growth, and the measurements were taken throughout the 7 days. The percentage growth inhibition (GI) of *G. boninense* growth was calculated using the following equation: GI (%) = [(colony diameter (cm) in control plate − colony diameter (cm) in treatment plate)/(colony diameter (cm) in control plate)] × 100. All data for the eight independent tests are presented as the mean ± standard deviation. The comparison of obtained values was analyzed using a statistical analysis software (SAS version 9.4) by one-way and two-way analyses of variance (ANOVA) followed by Tukey's test.[16] The significant value was considered when the p value was <0.05.

Oil Palm Plant Preparation for an *In Vivo* Nursery Trial. A total of 45 3-month-old oil palm seedlings (variety *Dura* × *Pisifera*) were obtained from Makmal Biji Cambah Rubber Industry Smallholders Development Authority (Sungkai, Perak, Malaysia). Each seedling was placed into a polybag (16 in. × 16 in.) containing top soil, organic material, and sand in a 3:2:1 (w:w) ratio.[17] The seedlings were watered daily to promote growth development in the 2B Glasshouse, Faculty of Agriculture, UPM, Malaysia.

Preparation of the Rubber Wood Block Inoculum. Rubber (*Hevea brasiliensis*) wood blocks (RWB) were cut into 6 cm × 6 cm × 6 cm pieces, drilled on each side, and air-dried under the sun. RWBs were soaked in distilled water for 24 h and then autoclaved at 121 °C for 20 min. For large-scale inoculum preparation, the primary culture was inoculated on MEA plates to obtain secondary cultures.[18] MEA (100 mL) was applied evenly over the surfaces of each RWB, which were autoclaved and cooled to room temperature (28 ± 2 °C). Following subculturing, the 7-day-old *G. boninense* culture was used for all subsequent RWB inoculations. Each RWB was inoculated with six pieces of mycelial discs (diameter of 1 cm) at six different sides of the RWB. The inoculated RWBs were incubated in a dark chamber for 3 months at room temperature.[18] Only RWBs that were completely covered by mycelia (i.e., showing active colonization) were used to infect the oil palm seedlings. For the disease trial, each seedling was carefully excavated from the polybag, and the bole was then placed directly on top of a fully colonized RWB inoculum. Next, the roots were dispersed to the sides of the RWB. The oil palm seedling together with the attached RWB inoculum was replanted into the polybag.

https://doi.org/10.1021/acsami.3c11697
ACS Appl. Mater. Interfaces XXXX, XXX, XXX−XXX

Experimental Design for the Antifungal Treatment. The antifungal treatment experiments were carried out in a completely random design (CRD) using non-inoculated seedlings, inoculated (untreated) seedlings, and seven treatments by a commercial hexaconazole fungicide, MOF-1201, UPMOF-1, UPMOF-2, Hex@MOF-1201, Hex@UPMOF-1, and Hex@UPMOF-2. For the hexaconazole-loaded MOF treatments (i.e., Hex@MOF-1201, Hex@UPMOF-1, and Hex@UPMOF-2), 3.0% hexaconazole was used as the active ingredient with five replicates. In a typical experiment, ∼500 mg of each treatment was pocketed in the soil on four sides. When the commercial treatment was being applied, the sample was diluted by a factor of 1:1000 [sample:water (*v*:*v*)] according to the prescription and applied directly to the soil. A total of 45 seedlings were used in this experiment. The treatments were first applied before inoculation ("pretreatment") and monthly ("post-treatment") thereafter for a total of 28 weeks. The seedlings were maintained by daily watering and provided NPK (nitrogen, phosphorus, and potassium) green fertilizer according to the standard procedures by the Malaysian Oil Palm Board.[19]

Disease Severity Index (DSI). The DSI was calculated every 2 weeks on the basis of the formula DSI = $[\Sigma(AB) \times 100]/(\Sigma B \times 4)$, where A is the disease class score (0−4) and B is the number of plants that exhibited disease per treatment.

RESULTS AND DISCUSSION

Synthesis of the Calcium L-Malate and Calcium D-Tartrate Frameworks: UPMOF-1 and -2, Respectively. The objective of this research program was to create environmentally sustainable agrichemical adjuvants that combine a high degree of selectivity, efficiency, and activity. As such, two types of low-molecular weight aliphatic plant acids, namely, L-malic and D-tartaric acid (Figure S1), were chosen as the organic linker building blocks to be linked with Ca-based clusters in the extended frameworks, UPMOF-1 and -2, respectively. As the solvent is known to play a critical role in the coordination behavior, connectivity, and dimensionality of Ca ions used to construct extended frameworks, the synthesis conditions were initially optimized by exploring both polar aprotic and polar protic solvents in their pure and mixed forms.[20,21] For solvothermal reactions that took place in pure or binary polar aprotic solvents, only amorphous products were obtained. When the reaction was performed in a pure polar protic solvent (i.e., water), a discrete metal complex was formed. Accordingly, single crystals of UPMOF-1 were solvothermally synthesized using a binary polar protic solvent system of water and ethanol [1:1 (*v*:*v*)] in 40% yield (Figure S2a). Optimization of the UPMOF-2 synthesis followed a strategy similar to that of UPMOF-1. Solvothermal reactions in pure polar aprotic solvents yielded amorphous powders, and when only water was used, a discrete metal complex was obtained. Single crystals of UPMOF-2 were, therefore, realized when using a binary solvent system of water and *N*,*N*′-dimethylformamide [DMF; 1:1 (*v*:*v*)] in 38% yield (Figure S2b).

Crystal Structures of UPMOF-1 and -2. SCXRD analysis revealed that UPMOF-1 crystallized in an orthorhombic system, space group $P2_12_12_1$ (No. 19), with the following lattice constants: a = 7.723(3) Å, b = 8.762(3) Å, and c = 29.287(8) Å (Table S1). The asymmetric unit of UPMOF-1 consists of three independent Ca^{2+} ions (i.e., Ca_1−Ca_3), three linkers (i.e., L-malate), and one uncoordinated water molecule (Figure S3). The presence of water around the coordination sites is a result of the high hydration energy of the Ca^{2+} metal centers.[22] L-Malate is observed to exhibit three different coordination modes. The hydroxyl O atoms in L-malate coordinate with both Ca_1 and Ca_3, while the O atoms from carboxylate groups coordinate to Ca_1 and Ca_2. Two O atoms, one each from the hydroxyl and carboxylate groups, coordinate with Ca_1 to form a five-membered ring (Figure S4). Two L-malate linkers act as bridges to connect the Ca_1 and Ca_2 building units. Ca_1−Ca_3 adopted coordination numbers of four, three, and two, respectively, which resulted in distorted geometries. Because of the orientation in which the Ca^{2+} centers were stitched together via the L-malate linkers, a three-dimensional framework composed of irregular pore channels was generated. Ca−O bond lengths were found to be in the range of 2.3−2.5 Å, and O−Ca−O angles were calculated to be between 64.2° and 167°, values that are in line with the coordination number and geometry of the Ca^{2+} atom in question (see Table S2). Topological analysis of UPMOF-1 was evaluated using ToposPro version 5.4.1.0.[23] During the analysis, the simplification method, "cluster", was used for the abstraction of both the L-malate linkers and Ca-based clusters. Accordingly, UPMOF-1 adopted a new topology, termed **mbr**, with a point symbol of $(4^2.6^4)(4^2.6^{10}.8^3)(6^6)$ due to the linkage of 6-c and 8-c Ca-based clusters with L-malate linkers serving as 3-c nodes (Figure S5).

UPMOF-2 also crystallizes in an orthorhombic system, space group $P2_12_12_1$ (No. 19), with the following lattice constants: a = 6.857(3) Å, b = 7.749(3) Å, and c = 12.060(5) Å. The asymmetric unit of UPMOF-2 has only one independent Ca^{2+} atom and one D-tartarate linker. The D-tartarate adopts one type of coordination mode from the O atom of its carboxylate group with the hydroxyl O atoms remaining uncoordinated (Figures S6 and S7). The reason for this is likely the high reaction temperature, which caused the deprotonation of the carboxylate groups first leading to fast binding with Ca^{2+} atoms.[24,25] The Ca−O bond lengths (∼2.3 Å) were similar to those calculated in UPMOF-1 (Table S3). The overall structure of UPMOF-2 is characterized by the one-dimensional Ca−tartarate rod building unit that produces rhombohedral channels that propagate along the b axis. UPMOF-2 exhibits an overall **gra** topology with the point symbol $(6^3)(6^9.8)$. For this topological determination, the D-tartarate linkers and Ca^{2+} sites serve as 3-c and 5-c nodes, respectively (Figure S8).

Structural Characterization. Prior to the structural characterization measurements, both UPMOF-1 and -2 were thoroughly washed to remove any unreacted starting material and/or impurities and then solvent-exchanged and activated to yield guest-free materials.

The crystallinity and bulk phase purity of the as-synthesized, solvent-exchanged, and activated samples were proven by powder X-ray diffraction (PXRD) analysis. Accordingly, the diffraction patterns for these samples of UPMOF-1 and -2 were in satisfactory agreement with the diffraction patterns simulated from their corresponding single-crystal structures (Figures S9 and S10). FT-IR spectroscopy measurements provided further support for the formation of bonds between each linker and the Ca^{2+} building units in the activated frameworks. In the spectra for the pure linkers, the characteristic absorption bands for the hydroxyl (e.g., ν_{-O-H} = 3700−3000 cm^{-1}) and carbonyl (e.g., $\nu_{-C=O}$ = 1750 cm^{-1}) functional groups were observed (Figures S11 and S12).[26] Upon comparison of the FT-IR spectra of the pure linkers to those of UPMOF-1 and -2, three important observations were noted. (i) The intensity of the carbonyl absorption band (e.g., $\nu_{-C=O}$ = 1750 cm^{-1}) decreased for UPMOF-1 and was absent for

https://doi.org/10.1021/acsami.3c11697
ACS Appl. Mater. Interfaces XXXX, XXX, XXX−XXX

UPMOF-2. This indicated coordination between the −C═O functional group for each of the linkers and Ca^{2+}.[27] (ii) Absorption bands appeared in the spectra of UPMOF-1 and -2 in the region from 1500 to 1250 cm^{-1}, which correspond to $-CH_3$ and $-CH_2-$ bending in the L-malate and D-tartarate linkers, respectively. This supports successful inclusion of the linkers within the frameworks. (iii) A shift in the −C−OH stretching absorption bands was observed from 1200−1020 cm^{-1} in the spectra of the pure linkers to ∼713 cm^{-1} in spectra of UPMOF-1 and -2. This shift indicated the formation of a new Ca−O−C coordination bond.

The architectural robustness of activated UPMOF-1 and -2 was assessed through a combination of TGA and N_2 adsorption isotherms at 77 K. The TGA traces for both materials exhibited similar three-stage thermal decomposition behavior (Figures S13 and S14). The first decomposition stage for UPMOF-1 and -2 began at 228 °C (13% weight loss) and 128 °C (4% weight loss), respectively, and was attributed to loss of water and solvent molecules adsorbed on the surface of both structures.[28,29] The higher temperature and percent weight loss observed for UPMOF-1's first decomposition stage were expected because of the presence of water molecules solvating the Ca^{2+} coordination sites as confirmed from the SCXRD analysis. UPMOF-1 and -2 were thermally stable up to 346 and 416 °C, respectively, at which point the second decomposition stage occurred with weight losses of 26% and 31%, respectively, that corresponded to the decomposition of coordinated hydroxyl and carboxylate groups from the terminal linkers.[7] The third and final stages of decomposition appeared at 531 °C (23% weight loss) and 588 °C (24% weight loss), respectively, for UPMOF-1 and -2. This final stage was due to framework decomposition. The remaining CaO residue was calculated to be 38.1% and 41.5% for UPMOF-1 and -2, respectively. Finally, N_2 adsorption isotherms at 77 K displayed type-III profiles for both UPMOF-1 and -2, indicating the bulk nonporosity of both materials (Figure S15).[30] This was expected and in line with previous literature reports on MOFs constructed from low-molecular weight (LMW) organic acids and/or alkaline earth metals.[7,31,32] Indeed, the flexibility of the L-malate and D-tartarate linkers can cause framework distortion toward dense, nonporous structures.[7,31,32]

The hydrolytic stability of MOFs is governed by many factors, including, but not limited to, the nature of the coordination bond between the metal and linker, the steric hindrance effect of the overall framework, and the porosity.[33,34] To better understand the response of these materials to water, UPMOF-1 and -2 were placed in aqueous solutions with a range of acidities. Accordingly, the structures of both materials disassembled and were completely soluble in acidic aqueous media (Figures S16−S25). This was expected as the Ca−linker bond is relatively weak, thereby allowing facile hydrolysis followed by linker displacement to form soluble calcium salts.[35,36] Furthermore, both UPMOF-1 and -2 were soluble in nitrate and sulfate solutions at all pH levels. However, in phosphate-based solutions (PBS and Na_3PO_4), UPMOF-1 and -2 were soluble under only acidic conditions (pH = 4−6) where, upon hydrolysis, the Ca^{2+} bonded with the PO_4^{2-} from the solvents to form the low-solubility $Ca_3(PO_4)_2$ salt.

Computational Simulations of Hexaconazole (Hex) Docking on UPMOF-1 and -2. Given the successful synthesis and characterization of UPMOF-1 and -2, the fact that both materials are constructed from nontoxic, naturally occurring, and eco-friendly building units (i.e., Ca^{2+} and LMW organic acids), and the disassembly of both UPMOFs in aqueous media, our attention turned toward understanding whether these frameworks could serve as adjuvants for agriculturally important fungicides, such as hexaconazole (Hex). The first step toward this understanding was to perform molecular docking simulations for Hex on (or within) UPMOF-1 and -2. Initially, it was clear that Hex was too large to be included or encapsulated within the internal pores of UPMOF-1 or -2. However, through computational simulations, Hex molecules, with differing conformational orientations, were found to interact with and reside on the outer surfaces of the two UPMOFs (Figure S26). It is noted that the molecular structure of Hex is highlighted by a N-containing five-membered heterocyclic ring that possesses a pyrrolic nitrogen (N−H), a pyridinic nitrogen (N), and a C−H bond, features that endow Hex with the ability to form multiple interactions with any nearby molecule. Accordingly, three types of interactions were identified between Hex and the surfaces of UPMOF-1 and -2 (Figure 2): (i) H-bonding, the most dominant and important interaction resulting from the O atoms from the UPMOF-1 and -2 linkers with the H atoms of Hex (i.e., $-NH_{Hex}\cdots O_{UPMOF}-Ca$ and $-C-H_{Hex}\cdots O_{UPMOF}-Ca$) [it is noted that the H-bond for Hex docking on UPMOF-1 (Hex@UPMOF-1) was stronger than that in Hex@UPMOF-2 given the presence of additional H-bonds]; (ii) metal acceptors, Hex's electron rich pyridinic N atom that provided active sites for the formation of metal−acceptor interactions, thereby forming a metal−acceptor interaction with the coordinatively unsaturated Ca atoms located on the surface of the UPMOFs; and (iii) electrostatic interactions (Table S4).

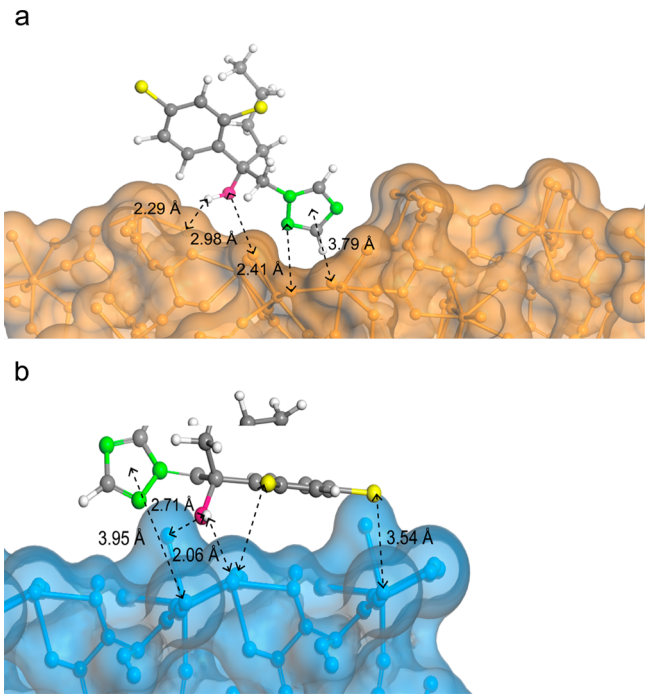

Figure 2. Docking simulation between Hex and UPMOF-1 and UPMOF-2. (a) Relevant host−guest interactions of Hex on the surface of UPMOF-1. (b) Relevant host−guest interactions of Hex on the surface of UPMOF-2. Hex is displayed as a ball-and-stick model (C, gray; N, green; O, pink; Cl, yellow; H, white), whereas the UPMOFs are in space-filling mode (UPMOF-1, orange; UPMOF-2, blue).

https://doi.org/10.1021/acsami.3c11697
ACS Appl. Mater. Interfaces XXXX, XXX, XXX−XXX

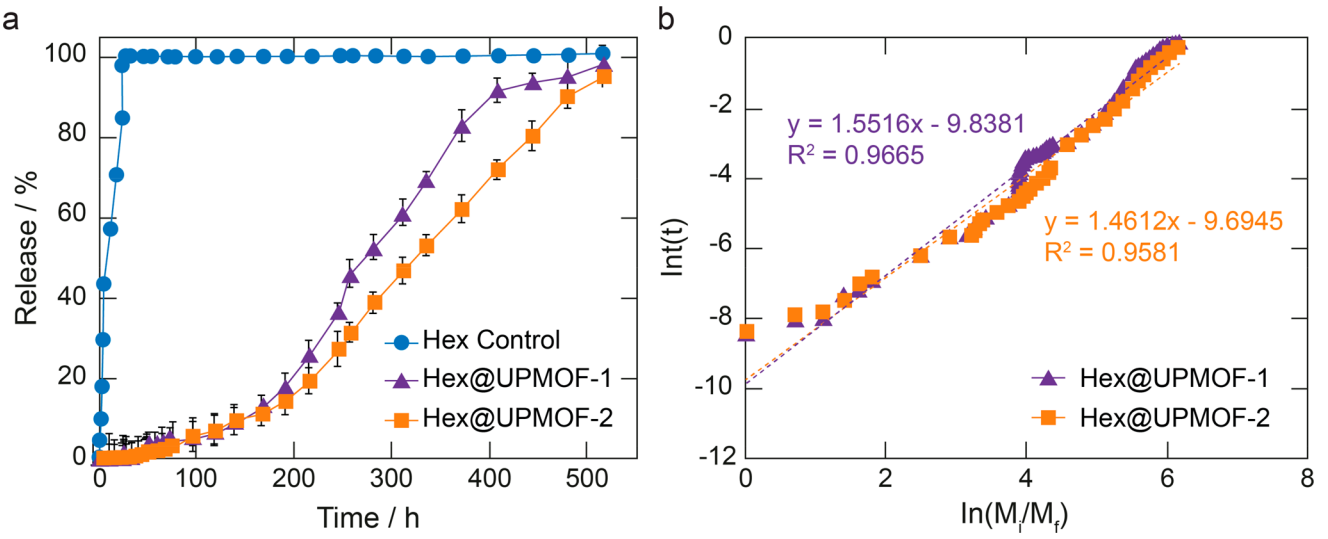

Figure 3. Cumulative release and kinetic profile of hexaconazole. (a) Hex (blue circles), Hex@UPMOF-1 (purple triangles), and Hex@UPMOF-2 (orange squares) released in a phosphate-buffered saline solution (PBS, 0.04 M, pH 7.4). (b) Release profiles for Hex@UPMOF-1 (purple triangles) and Hex@UPMOF-2 (orange squares) fitted to the mathematical Ritger and Peppas model.

Given these interactions, the binding affinity for docking Hex on UPMOF-1 (−5.0 kcal mol^{-1}) was stronger than that of docking on UPMOF-2 (−3.5 kcal mol^{-1}).[37] Overall from the simulations, it is clear that Hex can dock and be loaded onto both UPMOF-1 and -2 by forming stable host−guest interactions.[38]

Loading Hex on UPMOF-1 and -2. To experimentally load Hex on UPMOF-1 and -2, both MOFs were immersed in a Hex-containing ethanolic solution and microwave irradiated (100 W) at 90 °C for 3 min. Upon completion of microwave irradiation, the Hex@UPMOF-1 and -2 solids were filtered, and the supernatant was subjected to high-performance liquid chromatography (HPLC) to determine the efficiencies of loading (i.e., quantitative measurement of Hex remaining in the ethanolic solution) and docking (i.e., quantitative measurement of the weight of Hex added to the MOF solids) (Figures S27 and S28). From these measurements, slightly higher loading capacities and docking efficiencies were achieved for Hex@UPMOF-1 (63.04 ± 0.29% and 50.43 ± 0.17%, respectively) than for Hex@UPMOF-2 (62.02 ± 0.32% and 48.16 ± 0.14%, respectively).

From PXRD and SEM analysis, Hex@UPMOF-1 and Hex@UPMOF-2 retained the same crystal structures as the pristine unloaded UPMOF-1 and -2, respectively (Figures S29−S31). Through a combined SEM−energy dispersive X-ray spectroscopy and elemental analysis (EA) study, both Cl and N atoms that were derived from Hex molecules were observed in Hex@UPMOF-1 and Hex@UPMOF-2 samples (Figure S32 and Tables S6 and S7). To provide further spectroscopic evidence of Hex docking, the FT-IR spectra of Hex@UPMOF-1 and -2 were compared with the spectra for the parent, pristine UPMOF-1 and -2 and pure Hex (Figures S33 and S34). The spectra of both Hex@UPMOF-1 and -2 exhibited a broader absorption band between 3700 and 3000 cm^{-1}, which was attributed to a combination of −OH stretching from the hydroxyl and carboxylate functional groups in the linkers and −OH stretching from Hex.[11,15] The absorption band corresponding to −NH stretching (ν_{N-H} = 2650 cm^{-1}) in Hex disappeared in the Hex-loaded UPMOFs. This indicated that the −NH functional group formed H-bonds with the surfaces of UPMOF-1 and -2.[39] Furthermore, the characteristic aromatic C−N absorption band in Hex (ν_{C-N} = 1327 cm^{-1}) was observed in both spectra of Hex@UPMOF-1 and -2, thereby providing additional evidence of successful loading.[11] Additional absorption bands in the fingerprint region of the Hex-loaded MOF spectra further substantiated the loading (1390, 890, and 806 cm^{-1} for C−N stretching, C═C bending, and C−Cl stretching, respectively, in Hex).[15]

***In Vitro* Release of Hex from Hex@UPMOF-1 and -2 under Imitated Soil Conditions.** To investigate the release of Hex as a function of time, both Hex@UPMOF-1 and -2 were immersed in PBS that imitated soil conditions (0.04 M, pH 7.4). From these solutions, aliquots were taken at regular intervals from the supernatant and used to measure the Hex concentration via HPLC. Accordingly, the release profiles of Hex, as shown in Figure 3, demonstrate an S-curve with initial slow release before rapid faster release occurs. Specifically, in the first 24 h, <0.5% of the Hex was released from the UPMOFs. It was not until 282 and 336 h that at least 50% of Hex was released and >500 h that >98% and >95% of Hex were released from Hex@UPMOF-1 and -2, respectively. Given that the structures of both UPMOFs slowly disassemble upon their immersed in aqueous PBS medium, it is positive evidence that the Hex release profile from these UPMOFs mirrors this disassembly process. Finally, it is noted that the Hex release profiles from the UPMOFs are in stark contrast to the results of the control experiment of Hex in a dialysis tube alone, which exhibited a rapid release (>80%) within the first 24 h. We note that the slowest release of Hex (99.9%) reported in other studies was found to be at 86 h when chitosan nanoparticles attached with a cross-linking agent (i.e., sodium tripolyphosphate) were used.[11] Furthermore, Hex has been intercalated into a zinc/aluminum-layered double hydroxide using an ion exchange method, from which 62% of the intercalated Hex was released after 3000 min.[15] In this study, the low solubility of Hex in aqueous solutions helps to slow the interaction of the water/solvent molecules with Hex@UPMOF-1 and Hex@UPMOF-2.

To better understand the kinetics of the release of Hex from the UPMOFs, five kinetic models (i.e., first-order and second-

https://doi.org/10.1021/acsami.3c11697
ACS Appl. Mater. Interfaces XXXX, XXX, XXX−XXX

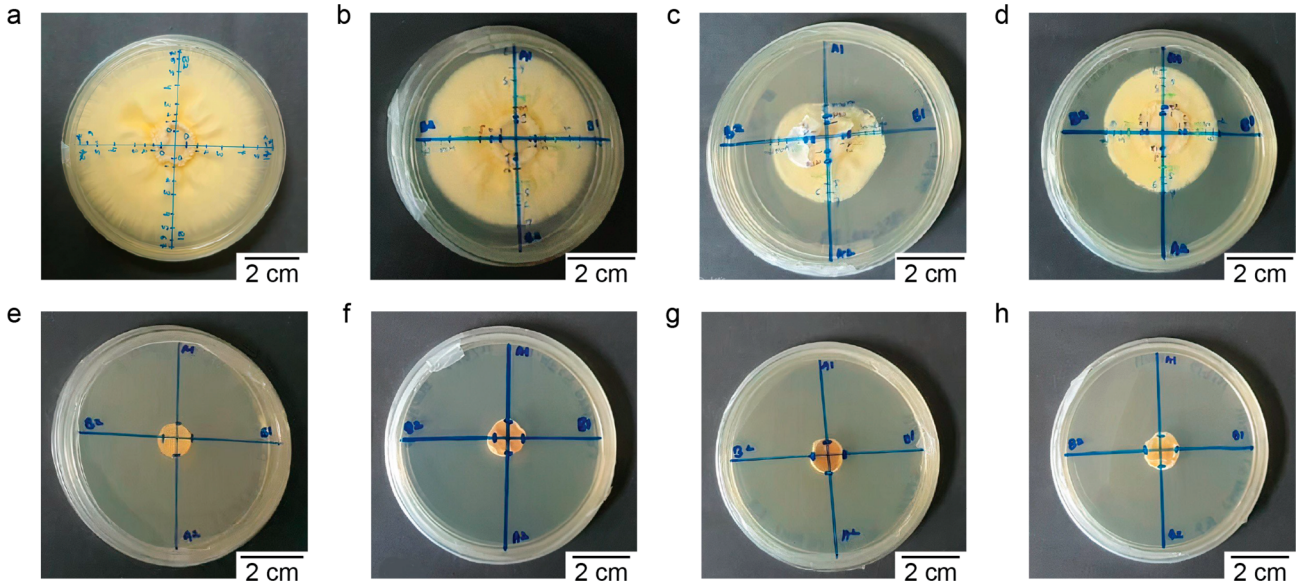

Figure 4. Antifungal effect on *G. boninense*: (a) control with no treatment, (b) MOF-1201, (c) UPMOF-1, (d) UPMOF-2, (e) commercial Hex, (f) Hex@MOF-1201, (g) Hex@UPMOF-1, and (h) Hex@UPMOF-2. As a representative example, the treatment concentration for all was 1 μg mL^{-1} at 29 °C, and as one can see, without treatment (a–d), *G. boninense* proliferates uncontrollably. Scale bars represent 2 cm.

order, Higuchi, Hixson–Crowel, and Ritger and Peppas) were used to fit the release data (Figure S35). On the basis of the calculated coefficient of determination (R^2), the Hex release data were best fit by the Ritger and Peppas model with an R^2 value of >0.95 (Figure 3b). This model categorizes the release into three possible transport mechanisms: (i) Fickian diffusion, (ii) non-Fickian diffusion, and (iii) case II diffusion.[40] The specific mechanism was then determined through two parameters (n and k), which represent the specific release mechanism and rate, respectively.[10,41,42] By applying the Ritger and Peppas model, the n (k) values for Hex@UPMOF-1 and -2 are 1.55 (2.29) and 1.55 (2.27), respectively, which means that the release of Hex from the UPMOFs follows case II type diffusion.

***In Vitro* Antifungal Activity Assay against *G. boninense*.** With the release of Hex from the UPMOFs established, attention turned toward studying the antifungal activity of these two MOF adjuvants. Specifically, antifungal activity was studied through a mycelial radial growth inhibition assay, also known as an "*in vitro*" direct contact assay.[11] The antifungal efficacy for the inhibition of *G. boninense* was evaluated by mixing potato dextrose agar (PDA) with distilled water alone as a control, the pristine MOFs (UPMOF-1 and -2 and MOF-1201), and the Hex-loaded MOFs (Hex@UPMOF-1, Hex@UPMOF-2, and Hex@MOF-1201) at different concentrations (0.05, 0.1, 1, 5, and 10 μg mL^{-1}). MOF-1201 was chosen as a second control as its composition is similar to those of UPMOF-1 and -2.[7,15] The inhibitory effect of pure Hex, Hex@UPMOF-1, Hex@UPMOF-2, and Hex@MOF-1201 on *G. boninense* was evaluated according to the inhibition rate, from which a higher inhibition rate equates to a more effective fungicide agent in combating the basal stem rot disease caused by *G. boninense* (Figure 4).[19] Accordingly, at a low concentration of 0.05 μg mL^{-1}, UPMOF-1, UPMOF-2, MOF-1201, and Hex@MOF-1201 displayed a negligible inhibitory effect and no significant difference with the control (i.e., no treatment; 6.27 cm) as maximum mycelial growth was measured at 5.32, 5.7, 5.18, and 5.1 cm, respectively (Table S8). As expected, pure Hex exhibited significantly better inhibition activity with 0 cm of mycelial growth of *G. boninense*. Hex@UPMOF-1 and Hex@UPMOF-2 both demonstrated significant inhibitory effects in which there was an absence of mycelial growth.

Following these initial results, the percent inhibition after 7 days was then calculated (Figure 5). Accordingly, pure Hex displayed a significant inhibitory effect beginning from 0.05 μg mL^{-1} until complete inhibition (100%) was reached at 10 μg mL^{-1}. Both Hex@UPMOF-1 and -2 demonstrated complete inhibition (100%) of *G. boninense* growth at the notably low concentration of 0.05 μg mL^{-1}. The pristine, Hex-free MOFs (UPMOF-1, UPMOF-2, and MOF-1201) displayed minimal ability to inhibit the growth (≤50%) of *G. boninense* starting at 0.05 μg mL^{-1}. Taken together, these findings point to the fact that the UPMOFs, as adjuvants, are effective in delivering the Hex fungicide against *G. boninense*.

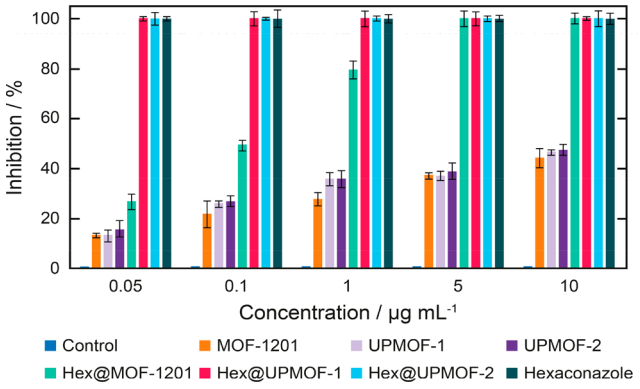

Figure 5. Percentage inhibition of radial growth on *G. boninense* as a function of concentration (micrograms per milliliter; day 7; 28 ± 2 °C) for no fungicide (blue), MOF-1201 (orange), UPMOF-1 (light purple), UPMOF-2 (dark purple), Hex@MOF-1201 (light green), Hex@UPMOF-1 (pink), Hex@UPMOF-2 (light blue), and pure Hex (dark green). Error bars represent standard deviations.

https://doi.org/10.1021/acsami.3c11697
ACS Appl. Mater. Interfaces XXXX, XXX, XXX–XXX

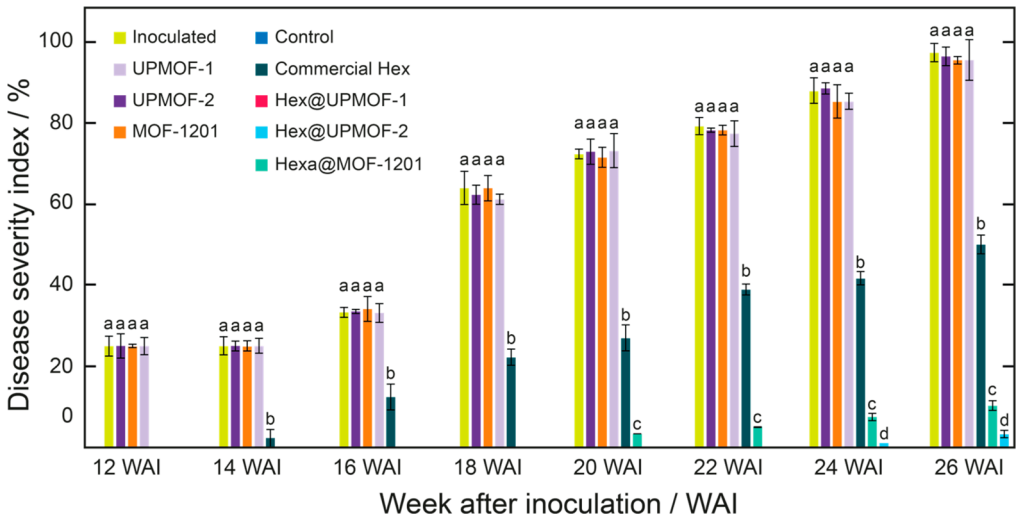

Figure 6. Disease severity index (DSI) in untreated and Hex-loaded MOF-treated oil palm seedlings for no fungicide (blue), MOF-1201 (orange), UPMOF-1 (light purple), UPMOF-2 (dark purple), Hex@MOF-1201 (light green), Hex@UPMOF-1 (pink), Hex@UPMOF-2 (light blue), and pure Hex (dark green). Error bars represent standard deviations. Means with the same letter in the same column are not significantly different according to the least significant difference (LSD; $p \geq 0.05$). The p value is for the analysis of variance (ANOVA). WAI = weeks after inoculation.

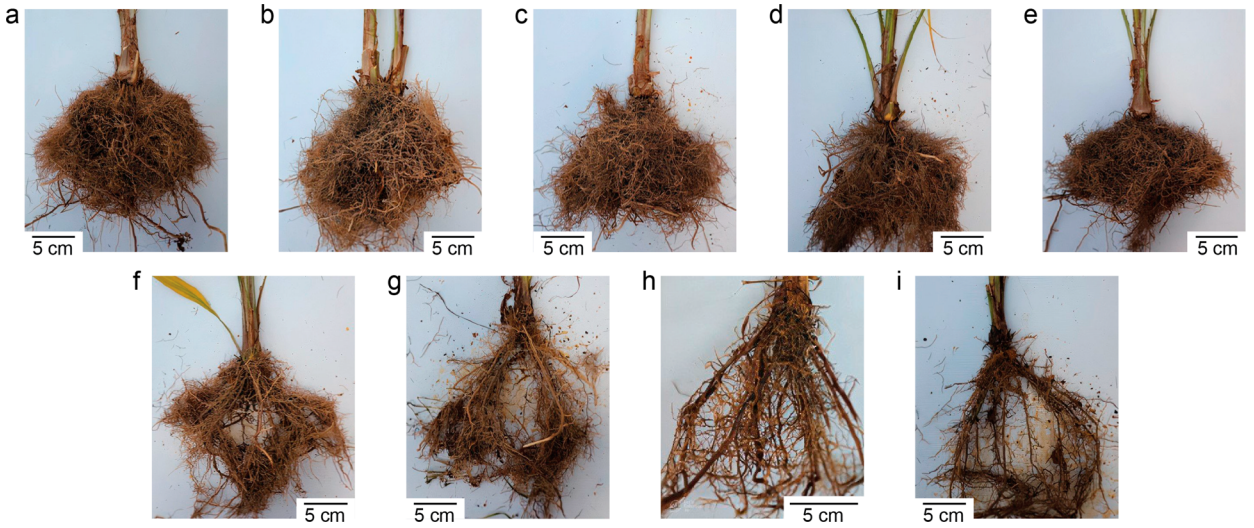

Figure 7. Roots of oil palm seedlings 26 weeks after inoculation (WAI): (a) healthy seedling, seedlings treated with (b) Hex@UPMOF-1, (c) Hex@UPMOF-2, (d) Hex@MOF-1201, (e) commercial Hex, (f) UPMOF-1, (g) UPMOF-2, and (h) MOF-1201, and (i) seedling inoculated with *G. boninense*. The scale bar is 5 cm.

***In Vivo* Oil Palm Plant Nursery Trial.** To demonstrate the practical applicability of Hex@UPMOF-1 and -2, we carried out a 26 week *in vivo* plant nursery trial. A total of 45 3-month-old oil palm seedlings (variety *Dura* × *Pisifera*) were first grown in separate polybags in a glasshouse. To prepare for the disease trial, each seedling was carefully excavated from its polybag and placed on rubber (*H. brasiliensis*) wood blocks (RWB) inoculated with *G. boninense* to infect the oil palm seedlings. The roots were dispersed to the sides of the RWB, and the oil palm seedling, together with the attached RWB, was replanted into the polybag.

The antifungal treatment experiments were then performed in a completely random design using non-inoculated seedlings, untreated inoculated seedlings, and inoculated seedings that were subjected to seven treatments each with commercially available Hex, UPMOF-1, UPMOF-2, MOF-1201, Hex@UPMOF-1, Hex@UPMOF-2, and Hex@MOF-1201. For the Hex-loaded MOF treatments (i.e., Hex@UPMOF-1, Hex@UPMOF-2, and Hex@MOF-1201), 3.0% Hex was used as the active ingredient, with five replicates. In a typical experiment, ~500 mg of each treatment was pocketed in the soil on four sides. When the commercial Hex treatment was being performed, the sample was diluted by a factor of 1:100 [sample:water (v:v)] according to the prescription and applied directly to the soil. The treatments were first applied before inoculation ("pretreatment") and maintained every 4 weeks ("post-treatment") thereafter for a total of 26 weeks. The seedlings were maintained by daily watering and by providing NPK (nitrogen, phosphorus, and potassium) green fertilizer according to the standard procedures of the Malaysian Palm Oil Board.[19] Monitoring the efficacy of the treatments was performed by scoring each of the plants for disease class on a scale of 0–4, from which the DSI could then be calculated.[18] From the data, no clear trend was observed 10 weeks after inoculation (WAI). At 12 WAI, a rapid 25% increase in the DSI for the inoculated seedlings and those seedlings treated

https://doi.org/10.1021/acsami.3c11697
ACS Appl. Mater. Interfaces XXXX, XXX, XXX−XXX

with the Hex-free pristine MOFs (UPMOF-1, UPMOF-2, and MOF-1201) was observed (Figure 6). Furthermore, at this 12 WAI stage, a significant difference was observed between the inoculated and Hex-free pristine MOF-treated seedlings and the seedlings that were treated with commercial Hex and Hex-loaded MOFs. Specifically, white mycelium was seen on the soil surface of the inoculated and Hex-free pristine MOF-treated seedlings (Figure S36a). At 16 WAI, the seedlings treated with commercial Hex (12.4% DSI) started to exhibit symptoms of *G. boninense* infection and the formation of white fungal "buttons" was detected on the soil of the inoculated and Hex-free pristine MOF-treated seedlings (Figure S36b). A 0% DSI was calculated at 16 WAI for those seedlings treated with the Hex-loaded MOFs with no noticeable difference among them. It was only at 26 WAI that the Hex-loaded MOF-treated seedlings began to show any appreciable infection, with DSI values of 0%, 3.3%, and 10.3% for Hex@UPMOF-1, Hex@UPMOF-2, and Hex@MOF-1201, respectively. At this stage of 26 WAI, the inoculated seedling had an extremely high DSI value of 97.3%.

It is worth noting that the rapid increase in DSI from 12 to 26 WAI suggested rapid disease progression in the untreated seedlings compared to those treated with the Hex-loaded MOFs. Those oil palm seedlings that were treated with the Hex-free, pristine MOFs produced negative *in vivo* results against *G. boninense* due to the absence of the active fungicide ingredient, which is relatively different than the *in vitro* results obtained (minor inhibition at 50 μg mL^{-1} toward *G. boninense*). Therefore, we can conclude that the Hex-free MOFs alone have minimal, practical antifungal activity and can inhibit mycelial growth only at early stages. On the contrary, the Hex-loaded MOF treatments were conclusively demonstrated to prevent disease progression in inoculated oil palm seedlings by suppressing the growth of *G. boninense* through the prolonged release of Hex.

Effects of Hex@UPMOF-1 and -2 on Oil Palm Seedling Roots. At the end of the experiment (26 WAI), the weights of the seedling roots were measured, and significant differences between each treatment were observed (Figure 7). Seedlings that were treated with Hex@UPMOF-1, Hex@UPMOF-2, Hex@MOF-1201, and commercial Hex were not significantly different from the healthy, non-inoculated seedlings (control). The largest weight was for the Hex@UPMOF-1-treated seedling (205.22 g) followed by the seedlings treated with Hex@UPMOF-2 (200.70 g), Hex@MOF-1201 (198.52 g), and commercial Hex (195.98 g) (Table 1). However, seedlings treated with pristine MOFs and untreated seedlings were significantly different from the control, where the weight of the roots was much smaller. Furthermore, the roots observed were less dense than the control. From this root assessment, Hex@UPMOF-1 was clearly the optimal treatment for protecting oil palm seedlings against basal stem rot infection. This finding points to the synergistic ability of the Hex-loaded UPMOFs not only to protect the oil palm seedlings via Hex but also to provide the helpful nutrients for plant growth through its disassembly into free Ca^{2+} and nontoxic organic molecules (linkers). Indeed, it is known that the addition of Ca^{2+} to soil promotes the formation of Ca^{2+} availability for precipitation with phosphorus, a process that supports balancing the phosphorus sorption mechanisms in plants.[43]

Table 1. Assessment of Oil Palm Seedling Plant Growth 7 Months after Inoculation

treatment	root mass[a] (g)
control	200.19 ± 5.59 a
inoculated	44.98 ± 1.82 c
commercial	195.98 ± 9.23 a
MOF-1201	89.89 ± 8.67 b
UPMOF-1	93.54 ± 1.00 b
UPMOF-2	90.23 ± 1.67 b
Hex@MOF-1201	198.52 ± 4.73 a
Hex@UPMOF-1	205.22 ± 4.04 a
Hex@UPMOF-2	200.70 ± 1.51 a

[a]Means followed by the same letter in the same column are not significantly different according to the LSD ($p \geq 0.05$). The letters a–c are statistical groupings, by which the values within those groupings are statistically similar. The p value is for the analysis of variance (ANOVA).

CONCLUSION

This study presents the synthesis and structural characterization of two new MOFs, termed UPMOF-1 and -2, from nontoxic, environmentally sustainable building blocks in Ca^{2+} and the LMW organic acids, L-malic acid and D-tartaric acid, respectively. Both UPMOF-1 and -2 were demonstrated to be effective adjuvants of the active fungicide hexaconazole (Hex). Given their tendency to disassemble in media that mimic soil conditions, the Hex-loaded UPMOFs, Hex@UPMOF-1 and -2, completely inhibited *G. boninense* growth (100%) in *in vitro* antifungal activity assays after 7 days even in low concentrations (0.05 μg mL^{-1}) as a result of the prolonged and sustained release of Hex ($\lesssim$500 h) as the MOFs disassembled. To demonstrate practical applicability, the Hex-loaded UPMOFs were subjected to a 26 week *in vivo* oil palm plant nursery trial, from which it was ascertained that the treatments with the Hex-loaded UPMOFs not only prevented disease progression but also contributed to seedling growth by providing additional nutrients to the soil (i.e., Ca^{2+}). This was further supported by the root weight differences observed between oil palm seedlings treated with the Hex-loaded UPMOFs. In the future, Hex@UPMOF-1 and -2 should be viewed as a micronutrient rich, viable, environmentally sustainable, and responsible treatment option for controlling basal stem rot disease in oil palms.

ASSOCIATED CONTENT

Data Availability Statement

The authors declare that all data supporting the findings of this study are available within the article and its Supporting Information or from the corresponding author upon reasonable request.

Supporting Information

The Supporting Information is available free of charge at https://pubs.acs.org/doi/10.1021/acsami.3c11697.

Single-crystal X-ray diffraction analysis, structural characterization of UPMOF-1 and -2, molecular docking simulation details, hexaconazole loading studies, *in vitro* release studies and kinetics, and inhibition of *G. boninense* and antifungal treatment (PDF)

Crystallographic data for UPMOF-1 (CIF)

Crystallographic data for UPMOF-2 (CIF)

https://doi.org/10.1021/acsami.3c11697
ACS Appl. Mater. Interfaces XXXX, XXX, XXX−XXX

AUTHOR INFORMATION

Corresponding Authors

Mohd Basyaruddin Abdul Rahman − *Foundry of Reticular Materials for Sustainability, Institute of Nanoscience and Nanotechnology, Universiti Putra Malaysia, Serdang 43400 Selangor, Malaysia; Department of Chemistry, Faculty of Science, Universiti Putra Malaysia, Serdang 43400 Selangor, Malaysia;* orcid.org/0000-0002-5665-2564; Email: basya@upm.edu.my

Kyle E. Cordova − *Foundry of Reticular Materials for Sustainability, Institute of Nanoscience and Nanotechnology, Universiti Putra Malaysia, Serdang 43400 Selangor, Malaysia; Department of Chemistry, Faculty of Science, Universiti Putra Malaysia, Serdang 43400 Selangor, Malaysia; Integrated Materials Systems (iMS) Research Unit, Advanced Research Centre, Royal Scientific Society, Amman 11941, Jordan;* orcid.org/0000-0002-4988-0497; Email: kyle.cordova@rss.jo

Authors

Nurul Farhana Ahmad Aljafree − *Foundry of Reticular Materials for Sustainability, Institute of Nanoscience and Nanotechnology, Universiti Putra Malaysia, Serdang 43400 Selangor, Malaysia; Department of Chemistry, Faculty of Science, Universiti Putra Malaysia, Serdang 43400 Selangor, Malaysia*

Mohamad Firdaus Ahmad − *Department of Plant Protection, Faculty of Agriculture, Universiti Putra Malaysia, Serdang 43400 Selangor, Malaysia*

Umar Abd Aziz − *Foundry of Reticular Materials for Sustainability, Institute of Nanoscience and Nanotechnology, Universiti Putra Malaysia, Serdang 43400 Selangor, Malaysia*

Mostafa Yousefzadeh Borzehandani − *Foundry of Reticular Materials for Sustainability, Institute of Nanoscience and Nanotechnology, Universiti Putra Malaysia, Serdang 43400 Selangor, Malaysia; Department of Chemistry, Faculty of Science, Universiti Putra Malaysia, Serdang 43400 Selangor, Malaysia*

Adila Mohamad Jaafar − *Foundry of Reticular Materials for Sustainability, Institute of Nanoscience and Nanotechnology, Universiti Putra Malaysia, Serdang 43400 Selangor, Malaysia; Centre of Foundation Studies for Agricultural Science, Universiti Putra Malaysia, Serdang 43400 Selangor, Malaysia*

Norhayu Asib − *Foundry of Reticular Materials for Sustainability, Institute of Nanoscience and Nanotechnology, Universiti Putra Malaysia, Serdang 43400 Selangor, Malaysia; Department of Plant Protection, Faculty of Agriculture, Universiti Putra Malaysia, Serdang 43400 Selangor, Malaysia*

Ha L. Nguyen − *Department of Chemistry, University of California, Berkeley, Berkeley, California 94720, United States;* orcid.org/0000-0002-4977-925X

Mohamed Ibrahim Mohamed Tahir − *Foundry of Reticular Materials for Sustainability, Institute of Nanoscience and Nanotechnology, Universiti Putra Malaysia, Serdang 43400 Selangor, Malaysia; Department of Chemistry, Faculty of Science, Universiti Putra Malaysia, Serdang 43400 Selangor, Malaysia*

Muhammad Alif Mohammad Latif − *Foundry of Reticular Materials for Sustainability, Institute of Nanoscience and Nanotechnology, Universiti Putra Malaysia, Serdang 43400 Selangor, Malaysia; Centre of Foundation Studies for Agricultural Science, Universiti Putra Malaysia, Serdang 43400 Selangor, Malaysia;* orcid.org/0000-0002-3345-0265

Complete contact information is available at: https://pubs.acs.org/10.1021/acsami.3c11697

Author Contributions

The manuscript was written through contributions of all authors. N.F.A.A.: methodology, formal analysis, and writing of the original draft. M.F.A.: methodology and formal analysis. U.A.A.: investigation. M.Y.B.: software. A.M.J.: supervision. N.A.: resources and supervision. H.L.N.: formal analysis. M.I.M.T.: validation. M.A.M.L.: software and visualization. K.E.C.: conceptualization, visualization, and reviewing and editing. M.B.A.R.: conceptualization, project administration, funding acquisition, and supervision. All authors have approved the final version of the manuscript.

Funding

This work was supported by Ministry of Science, Technology and Innovation of Malaysia (MOSTI - IF09180O1033, 5450825). K.E.C. is grateful for support from the Newton-Khalidi Fund and the Royal Academy of Engineering's Transforming Systems through Partnership Program (TSP2021/100001).

Notes

The authors declare the following competing financial interest(s): A patent has been filed: Universiti Putra Malaysia (patent applicant), Mohd Basyaruddin Abdul Rahman (M.B.A.R.), Norhayu Asib (N.A.), and Nurul Farhana Ahmad Aljafree (N.F.A.A.) (inventors), MyIPO application serial no. PI 2022002029 with priority date 20 April 2022, relating to a calcium-based metal organic framework composition encapsulating a fungicide azole group and its method of preparation thereof. The remaining authors declare no competing financial interests.

ACKNOWLEDGMENTS

The authors thank Prof. Omar M. Yaghi (University of California, Berkeley) for helpful insights.

ABBREVIATIONS

CRD, completely random design; DSI, disease severity index; GI, growth inhibition; Hex, hexaconazole; LMW, low molecular weight; MEA, malt extract sugar; MEB, malt extract broth; NPK, nitrogen, phosphorus, and potassium; PDA, potato dextrose agar; RWB, rubber wood block; WAI, weeks after inoculation

REFERENCES

(1) Rojas, S.; Rodriguez-Dieguez, A.; Horcajada, P. Metal-Organic Frameworks in Agriculture. *ACS Appl. Mater. Interfaces* **2022**, *14*, 16983−17007.

(2) Foley, J. A.; Ramankutty, N.; Brauman, K. A.; Cassidy, E. S.; Gerber, J. S.; Johnston, M.; Mueller, N. D.; O'Connell, C.; Ray, D. K.; West, P. C.; Balzer, C.; Bennett, E. M.; Carpenter, S. R.; Hill, J.; Monfreda, C.; Polasky, S.; Rockström, J.; Sheehan, J.; Siebert, S.; Tilman, D.; Zaks, D. P. M. Solutions for a Cultivated Planet. *Nature* **2011**, *478*, 337−342.

(3) *The future of food and agriculture: Trends and challenges*; Food and Agriculture Organization of the United Nations: Rome, 2017.

(4) Aktar, W.; Sengupta, D.; Chowdhury, A. Impact of Pesticide Use in Agriculture: Their benefits and hazards. *Interdiscp. Toxicol.* **2009**, *2*, 1−12.
(5) Yin, J.; Wang, Y.; Gilbertson, L. M. Opportunities to Advance Sustainable Design of Nano-enabled Agriculture Identified through a Literature Review. *Environ. Sci. Nano* **2018**, *5*, 11−26.
(6) Diercks, C. S.; Liu, Y.; Cordova, K. E.; Yaghi, O. M. The Role of Reticular Chemistry in the Design of CO_2 Reduction Catalysts. *Nat. Mater.* **2018**, *17*, 301−307.
(7) Yang, J.; Trickett, C. A.; Alahmadi, S. B.; Alshammari, A. S.; Yaghi, O. M. Calcium $_L$-Lactate Frameworks as Naturally Degradable Carriers for Pesticides. *J. Am. Chem. Soc.* **2017**, *139*, 8118−8121.
(8) Sheldrick, G. M. Crystal Structure Refinement with SHELXL. *Acta Crystallogr. Sect. C Struct. Chem.* **2015**, *71*, 3−8.
(9) Macrae, C. F.; Sovago, I.; Cottrell, S. J.; Galek, P. T. A.; McCabe, P.; Pidcock, E.; Platings, M.; Shields, G. P.; Stevens, J. S.; Towler, M.; Wood, P. A. Mercury 4.0: From Visualization to Analysis, Design and Prediction. *J. Appl. Crystallogr.* **2020**, *53*, 226−235.
(10) Siepmann, J.; Peppas, N. A. Modeling of Drug Release from Delivery Systems Based on Hydroxypropyl Methylcellulose (HPMC). *Adv. Drug Delivery Rev.* **2001**, *48*, 139−157.
(11) Maluin, F.; Hussein, M.; Yusof, N.; Fakurazi, S.; Abu Seman, I.; Zainol, H.; Nur, H.; Daim, L. Enhanced Fungicidal Efficacy on: *Ganoderma boninense* by Simultaneous Co-delivery of Hexaconazole and Dazomet from Their Chitosan Nanoparticles. *RSC Adv.* **2019**, *9*, 27083−27095.
(12) Maluin, F. N.; Hussein, M. Z.; Yusof, N. A.; Fakurazi, S.; Idris, A. S.; Hilmi, N. H. Z.; Daim, L. D. J. A Potent Antifungal Agent for Basal Stem Rot Disease Treatment in Oil Palms Based on Chitosan-Dazomet Nanoparticles. *Int. J. Mol. Sci.* **2019**, *20*, 2247−2262.
(13) Patel, S.; Bajpai, J.; Saini, R.; Bajpai, A. K.; Acharya, S. Sustained Release of Pesticide (Cypermethrin) from Nanocarriers : An Effective Technique for Environmental and Crop Protection. *Process Saf. Environ. Prot.* **2018**, *117*, 315−325.
(14) Chan, Y. S.; Chong, K. P. Novel Media for Cultivation of Fruiting Body of *Ganoderma boninense* for Medicinal Benefits. *ASM Sci. J.* **2019**, *12*, 11−16.
(15) Mustafa, I. F.; Hussein, M. Z.; Saifullah, B.; Idris, A. S.; Hilmi, N. H. Z.; Fakurazi, S. Synthesis of (Hexaconazole-Zinc/Aluminum-Layered Double Hydroxide Nanocomposite) Fungicide Nanodelivery System for Controlling Ganoderma Disease in Oil Palm. *J. Agric. Food Chem.* **2018**, *66*, 806−813.
(16) Nassiri, M.; Elahi Torshizi, M.; Ghovvati, S.; Doosti, M. Evaluation of Different Statistical Methods Using SAS Software: An *In Silico* Approach for Analysis of Real-Time PCR Data. *J. Appl. Stat.* **2018**, *45*, 306−319.
(17) Obeng, J.; Agyei-Dwarko, D.; Teinor, P.; Danso, I.; Lutuf, H.; Lekete-Lawson, E.; Ablormeti, F. K.; Eddy-Doh, M. A. Bioactivity of an Organic Farming Aid with Possible Fungistatic Properties against Some Oil Palm Seedling Foliar Pathogens. *Sci. Rep.* **2023**, *13*, 1280.
(18) Parvin, W.; Govender, N.; Othman, R.; Jaafar, H.; Rahman, M.; Wong, M.-Y. Phenazine from *Pseudomonas aeruginosa* UPMP3 Induced the Host Resistance in Oil Palm (*Elaeis guineensis* Jacq.)-*Ganoderma boninense* Pathosystem. *Sci. Rep.* **2020**, *10*, 15621.
(19) Keni, M. F.; Zainuddin, N.; Masri, M. M. M. Improving the Growth Performance of Oil Palm Seedlings by Mixtures of Organic and Chemical Fertilisers. *J. Oil Palm Res.* **2022**, *35*, 147−156.
(20) Gropp, C.; Canossa, S.; Wuttke, S.; Gandara, F.; Li, Q.; Gagliardi, L.; Yaghi, O. M. Standard Practices of Reticular Chemistry. *ACS Cent. Sci.* **2020**, *6*, 1255−1273.
(21) Furukawa, H.; Cordova, K. E.; O'Keeffe, M.; Yaghi, O. M. The Chemistry and Aplications of Metal-Organic Frameworks. *Science* **2013**, *341*, 1230444.
(22) Xian, S.; Lin, Y.; Wang, H.; Li, J. Calcium-Based Metal-Organic Frameworks and Their Potential Applications. *Small* **2021**, *17*, 2005165.
(23) Blatov, V. A.; Shevchenko, A. P.; Proserpio, D. M. Applied Topological Analysis of Crystal Structures with the Program Package Topospro. *Cryst. Growth Des.* **2014**, *14*, 3576−3586.
(24) Liu, J.; Wang, D.; Xu, X.; Li, H.; Zhao, J.; Chen, L. Multi-Nuclear Rare-Earth-Implanted Tartaric Acid-Functionalized Seleno-tungstates and Their Fluorescent and Magnetic Properties. *Inorg. Chem.* **2021**, *60*, 2533−2541.
(25) Rieger, A.; Sax, C.; Bauert, T.; Wäckerlin, C.; Ernst, K. H. Chiral Molecules Adsorbed on a Solid Surface: Tartaric acid Diastereomers and Their Surface Explosion on Cu(111). *Chirality* **2018**, *30*, 369−377.
(26) Ke, F.; Peng, C.; Zhang, T.; Zhang, M.; Zhou, C.; Cai, H.; Zhu, J.; Wan, X. Fumarate-Based Metal-Organic Frameworks as a New Platform for Highly Selective Removal of Fluoride from Brick Tea. *Sci. Rep.* **2018**, *8*, 939.
(27) Mazaj, M.; et al. Spectroscopic Studies of Structural Dynamics Induced by Heating and Hydration: A Case of Calcium-Terephthalate Metal-Organic Framework. *J. Phys. Chem. C* **2013**, *117*, 7552−7564.
(28) Sun, J.; Huang, T.; Yin, Q.; Li, L.; Liu, T.-F.; Huang, X.-S.; Cao, R. Tuning the Structure and Hydrolysis Stability of Calcium Metal-Organic Frameworks through Integrating Carboxylic/Phosphinic/Phosphonic Groups in Building Blocks. *Cryst. Growth Des.* **2020**, *20*, 8021−8027.
(29) Almáši, M.; Zeleňák, V.; Gyepes, R.; Zauška, Ľ.; Bourrelly, S. A Series of Four Novel Alkaline Earth Metal-Organic Frameworks Constructed of Ca(II), Sr(II), Ba(II) Ions and Tetrahedral MTB Linker: Structural Diversity, Stability Study and Low/High-Pressure Gas Adsorption Properties. *RSC Adv.* **2020**, *10*, 32323−32334.
(30) Bingel, L. W.; Walton, K. S. Surprising Use of the Business Innovation Bass Diffusion Model to Accurately Describe Adsorption Isotherm Types I, III, and V. *Langmuir* **2023**, *39*, 4475−4482.
(31) Wang, S.; Xhaferaj, N.; Wahiduzzaman, M.; Oyekan, K.; Li, X.; Wei, K.; Zheng, B.; Tissot, A.; Marrot, J.; Shepard, W.; Martineau-Corcos, C.; Filinchuk, Y.; Tan, K.; Maurin, G.; Serre, C. Engineering Structural Dynamics of Zirconium Metal-Organic Frameworks Based on Natural C_4 Linkers. *J. Am. Chem. Soc.* **2019**, *141*, 17207−17216.
(32) Fromm, K. M. Chemistry of Alkaline Earth Metals: It Is Not All Ionic and Definitely Not Boring! *Coord. Chem. Rev.* **2020**, *408*, 213193.
(33) Song, D.; Bae, J.; Ji, H.; Kim, M. B.; Bae, Y. S.; Park, K. S.; Moon, D.; Jeong, N. C. Coordinative Reduction of Metal Nodes Enhances the Hydrolytic Stability of a Paddlewheel Metal-Organic Framework. *J. Am. Chem. Soc.* **2019**, *141*, 7853−7864.
(34) Xue, W.; Wang, J.; Huang, H.; Mei, D. Structural and Hydrolytic Stability of Coordinatively Unsaturated Metal-Organic Frameworks M_3 $(BTC)_2$ (M = Cu, Co, Mn, Ni, and Zn): A Combined DFT and Experimental Study. *J. Phys. Chem. C* **2021**, *125*, 5832−5847.
(35) Liu, X.; Wang, X.; Kapteijn, F. Water and Metal-Organic Frameworks: From Interaction toward Utilization. *Chem. Rev.* **2020**, *120*, 8303−8377.
(36) Kalmutzki, M. J.; Diercks, C. S.; Yaghi, O. M. Metal-Organic Frameworks for Water Harvesting from Air. *Adv. Mater.* **2018**, *30*, 1704304.
(37) Chopra, N.; Kaur, D.; Chopra, G. Nature and Hierarchy of Hydrogen-Bonding Interactions in Binary Complexes of Azoles with Water and Hydrogen Peroxide Data Sets. *ACS Omega* **2018**, *3*, 12688−12702.
(38) Halder, S.; Barma, A.; Rizzoli, C.; Ghosh, P.; Roy, P. Density Functional Theory Analysis of Host-Guest Interactions in Cu(II)-Based Metal-Organic Frameworks for Pesticide Detection. *ACS Appl. Nano Mater.* **2019**, *2*, 5469−5474.
(39) Darlis, D.; Jalloh, M. B.; Chin, C. F. S.; Basri, N. K. M.; Besar, N. A.; Ahmad, K.; Rakib, M. R. M. Exploring the Potential of *Bornean polypore* Fungi as Biological Control Agents against Pathogenic *Ganoderma boninense* Causing Basal Stem Rot in Oil Palm. *Sci. Rep.* **2023**, *13*, 10316.
(40) Ritger, P. L.; Peppas, N. A. A Simple Equation for Description of Solute Release II. Fickian and Anomalous Release from Swellable Devices. *J. Controlled Release* **1987**, *5*, 37−42.

https://doi.org/10.1021/acsami.3c11697
ACS Appl. Mater. Interfaces XXXX, XXX, XXX−XXX

(41) Sinclair, G. W.; Peppas, N. A. Analysis of Non-Fickian Transport in Polymers Using Simplified Exponential Expressions. *J. Membr. Sci.* **1984**, *17*, 329−331.
(42) Peppas, N. A.; Sahlin, J. J. A Simple Equation for the Description of Solute Release. III. Coupling of Diffusion and Relaxation. *Int. J. Pharm.* **1989**, *57*, 169−172.
(43) Penn, C.; Camberato, J. A Critical Review on Soil Chemical Processes that Control How Soil pH Affects Phosphorus Availability to Plants. *Agriculture* **2019**, *9*, 120.

https://doi.org/10.1021/acsami.3c11697
ACS Appl. Mater. Interfaces XXXX, XXX, XXX−XXX